



Ecological speciation in sympatric palms: 3. Genetic map reveals genomic islands underlying species divergence in *Howea*

Papadopoulos, Alexander S. T.; Igea, Javier; Dunning, Luke T; Osborne, Owen; Quan, Xueping; Pellicer, Jaume; Turnbull, Colin; Hutton, Ian; Baker, William J.; Butlin, Roger K.; Savolainen, Vincent

Evolution

DOI:

[10.1111/evo.13796](https://doi.org/10.1111/evo.13796)

Published: 01/09/2019

Peer reviewed version

[Cyswllt i'r cyhoeddiad / Link to publication](#)

Dyfyniad o'r fersiwn a gyhoeddwyd / Citation for published version (APA):

Papadopoulos, A. S. T., Igea, J., Dunning, L. T., Osborne, O., Quan, X., Pellicer, J., Turnbull, C., Hutton, I., Baker, W. J., Butlin, R. K., & Savolainen, V. (2019). Ecological speciation in sympatric palms: 3. Genetic map reveals genomic islands underlying species divergence in *Howea*. *Evolution*, 73(9), 1986-1995. <https://doi.org/10.1111/evo.13796>

Hawliau Cyffredinol / General rights

Copyright and moral rights for the publications made accessible in the public portal are retained by the authors and/or other copyright owners and it is a condition of accessing publications that users recognise and abide by the legal requirements associated with these rights.

- Users may download and print one copy of any publication from the public portal for the purpose of private study or research.
- You may not further distribute the material or use it for any profit-making activity or commercial gain
- You may freely distribute the URL identifying the publication in the public portal ?

Take down policy

If you believe that this document breaches copyright please contact us providing details, and we will remove access to the work immediately and investigate your claim.

1 **BRIEF COMMUNICATION**

2

3 **Ecological speciation in sympatric palms: 3. Genetic map reveals genomic islands underlying**
4 **species divergence in *Howea***

5

6 **Abstract**

7 Although it is now widely accepted that speciation can occur in the face of continuous gene flow,
8 with little or no spatial separation, the mechanisms and genomic architectures that permit such
9 divergence are still debated. Here, we examined speciation in the face of gene flow in the *Howea*
10 palms of Lord Howe Island, Australia. We built a genetic map using a novel method applicable to
11 long-lived tree species, combining it with double digest restriction-site associated DNA sequencing
12 of multiple individuals. Based upon various metrics, we detected 46 highly differentiated regions
13 throughout the genome, four of which contained genes with functions that are particularly relevant
14 to the speciation scenario for *Howea*, specifically salt and drought tolerance.

15

16 **Introduction**

17 We investigated the genomic basis of speciation in *Howea* palms, which is a genus of only two
18 species endemic to a minute oceanic island, Lord Howe Island (LHI), in the Tasman sea. LHI sits
19 600 km off mainland Australia and is less than 16 km², meaning that for any pair of endemic sister
20 species that have diverged within the lifetime of the island (6.9 my), an allopatric phase in their
21 divergence is unlikely (Savolainen *et al.* 2006; Papadopulos *et al.* 2011). Hence, *Howea* is a solid
22 example of speciation in sympatry (Savolainen *et al.* 2006; Coyne 2011; Papadopulos *et al.* 2011,
23 2019). Furthermore, it has been hypothesised that the two *Howea* species diverged in sympatry as a
24 result of ecological speciation facilitated by soil adaptation and a shift in flowering phenology (Fig.
25 1; Savolainen *et al.* 2006; Babik *et al.* 2009; Papadopulos *et al.* 2011, 2013b, 2014; Hipperson *et al.*
26 2016). *Howea* is widespread on LHI, although *H. belmoreana* is restricted to the older volcanic
27 rocks whereas *H. forsteriana* is found predominantly on Pleistocene calcareous deposits
28 (calcareous) around the coast (Savolainen *et al.* 2006; Woodroffe *et al.* 2006; Papadopulos *et al.*
29 2013). Marked flowering time differences between the species indicate that prezygotic isolation is
30 now strong and current levels of gene flow are low (Savolainen *et al.* 2006; Babik *et al.* 2009;
31 Dunning *et al.* 2016; Hipperson *et al.* 2016; Papadopulos *et al.* 2019). Indirect evidence of post-
32 zygotic isolation due to selection against juvenile hybrids supports the hypothesis that divergent
33 selection has influenced the speciation process (Hipperson *et al.* 2016). Given that the distributions
34 of *Howea* palms overlap extensively and that *Howea* is wind pollinated, speciation is likely to have
35 occurred in the face of gene flow, which has reduced quickly as divergence progressed (Savolainen

36 *et al.* 2006; Babik *et al.* 2009; Papadopoulos *et al.* 2011, 2013, 2014, 2019). Here, we built a genetic
37 map using a novel method applicable to long-lived tree species, combining it with double digest
38 restriction-site associated DNA sequencing of multiple individuals, and we then examined the
39 landscape of genomic differentiation that has arisen during and after speciation in *Howea* palms.

40

41 **Material and Methods**

42

43 DNA EXTRACTION

44

45 For linkage mapping, a single, wild *H. belmoreana* tree was selected on LHI, and leaf tissue was
46 collected and preserved in silica gel. Ninety-four immature seeds were collected from this tree,
47 dissected, and the endosperm tissue was removed and preserved in RNAlater (Sigma-Aldrich).
48 Genomic DNA was then extracted using CTAB (Doyle & Doyle 1987) and purified using a
49 caesium chloride gradient and dialysis. DNA samples were further cleaned and concentrated using
50 DNeasy Mini spin columns (Qiagen). For the genome scan, leaf tissue was collected and preserved
51 in silica gel from 42 *H. belmoreana* and 54 *H. forsteriana* individuals sampled at Far Flats, a plot
52 on LHI where both species co-occur (Papadopoulos *et al.* 2019). For shotgun sequencing, a single,
53 wild collected *H. forsteriana* individual was used. Genomic DNA was extracted from these 97
54 individuals using DNeasy Plant Mini kits (Qiagen).

55

56 GENOTYPING AND LINKAGE MAP

57 Double digest RAD-sequencing (ddRAD) was performed following Papadopoulos *et al.* (2019). For
58 the map, we genotyped a mother tree and 94 of its seeds. During the formation of the female
59 megagametophyte a single cell undergoes meiosis and programmed cell death eliminates three of
60 the four descendent haploid spores (Fig. S1). Three sequential mitotic nuclear divisions take place
61 in the remaining megaspore to produce eight nuclei. Cellular division produces seven cells that
62 make up the embryo sac, one of which – the central cell - contains two polar nuclei (Sundaresan &
63 Alandete-Saez 2010). When fertilised, this homo-diploid cell develops into the triploid endosperm
64 containing a single copy of the paternal genome and two identical copies of the maternal genome.
65 Identification of which maternal allele is inherited by the offspring at any given heterozygous
66 position in the mother was achieved by ddRAD sequencing of the maternal and endosperm tissue.
67 The 2:1 ratio of maternal to paternal alleles is maintained in the relative read depth of alleles at each
68 locus in the endosperm, allowing the maternally inherited allele at each locus to be determined in
69 each seed sample (Fig. S1). The raw sequencing data were processed and individuals genotyped
70 using components of the *STACKS* (Catchen *et al.* 2011) pipeline, *perl* and *R* scripts (R Development

71 Core Team 2019). The ‘process-radtags’ component of *STACKS* was used to de-multiplex the
72 barcoded samples in each library, remove tags of low quality, with ambiguous barcodes or missing
73 base calls, and truncate each sequence to 95 bp. The paired ends of each read were then merged into
74 a single contiguous sequence to minimise the inclusion of paralogous sequences in the same RAD
75 loci in subsequent steps. The genotyping process was composed of four main steps: (i) construction
76 of a reliable, high coverage catalogue of heterozygous sites in the maternal tree; (ii) genotyping of
77 endosperm tissue at these sites; (iii) addition of loci/haplotypes present in trees from the LHI site to
78 the maternal catalogue; and (iv) genotyping of the wild trees. First (i), to remove highly similar
79 clusters of *STACKS* and error prone loci from the maternal dataset the *STACKS* pipeline was run
80 using at least five exactly matching reads to create a stack, allowing one mismatch between stacks
81 to create a locus, allowing up to 200 stacks to form a single locus, disabling the deleveraging
82 algorithm and disabling haplotype calling from secondary reads. Reads assigned to loci composed
83 of more than two haplotypes were then removed from the dataset. The remaining reads were then
84 processed using the *denovo_map.pl* perl wrapper for *STACKS* to generate a catalogue of loci and
85 haplotypes present in the mother using at least 50 exactly matching reads to create a stack and
86 allowing three mismatches between stacks to create a locus. (ii) Reads for each endosperm tissue
87 were assembled into loci using *USTACKS* (minimum depth to create a stack = 10, mismatches = 3)
88 and these were then mapped to the maternal catalogue using *SSTACKS*. For all heterozygous loci in
89 the mother, the two haplotypes in the endosperms were randomly assigned as an A or B allele and
90 the read depths of haplotypes were extracted for each seed using custom *perl* scripts. To determine
91 the maternally inherited allele (A or B) in each seed, the relative read depth of the A allele at each
92 locus (read depth of A/read depth of A + B) was analysed using the *kmeans* clustering algorithm in
93 R with 4 predefined clusters (corresponding to triploid genotypes of AAA = 1.00, AAB = 0.66,
94 BBA = 0.33 and BBB = 0.00). (iii) To expand the catalogue to encompass haplotypes present in
95 both *Howea* species, the Far Flats samples were assembled into loci using *USTACKS* (-m20, -M3)
96 and these stacks were merged into the existing catalogue allowing 3 mismatches between loci in
97 different individuals. (iv) To genotype the Far Flats individuals, loci were assembled with lower
98 coverage in *USTACKS* (-m5, -M3) and these stacks were mapped to the catalogue loci. For the
99 genome scan analyses, haplotypes of these individuals were extracted for loci included in the
100 linkage map. Genotypic data for the *H. belmoreana* seeds were initially processed using the *R/qtl*
101 (Broman *et al.* 2003) package. Four individuals were excluded due to high levels of missing data.
102 After exclusion of these samples, loci with more than 22 missing genotypes out of 90 progeny were
103 also removed from further analysis. The remaining 3,772 loci were phased and assembled into
104 linkage groups using the *formlinkagegroups* function with a minimum logarithm of odds threshold
105 of 7.0 and maximum recombination fraction of 0.25. The loci within each assembled linkage group

106 were then ordered in *JoinMap* v4.1 (Kyazma) using the regression mapping algorithm (three
107 rounds), and inter-marker distances were calculated in centimorgans (cM) using the Kosambi
108 mapping function. The mean coverage of mapped loci was 1,117 reads in the mother (s.d. +/- 1,145)
109 and 176 (s.d. +/- 89) in the endosperm. Unequivocal homozygote genotypes accounted for 51% of
110 endosperm allele calls, 32% of calls were derived from proportional differences between alleles and
111 17% were treated as missing data.

112

113 IDENTIFYING GENOMIC ISLANDS

114 Differentiation (i.e., F_{ST} ; Weir & Cockerham 1984) between *H. belmoreana* and *H. forsteriana* was
115 calculated at each ddRAD locus using the *diveRsity* package in *R* (Keenan *et al.* 2013). Divergence
116 (d_{XY}) was also calculated for each locus using equation 10.20 of Nei (1987). Genome-wide
117 distributions of F_{ST} and d_{XY} were generated using a local Gaussian kernel smoothing technique
118 within each chromosome (Hohenlohe *et al.* (2010). Kernel smoothing was performed using the
119 *ksmooth* function in *R* with a bandwidth value of 2 cM, defined as the standard deviation of the
120 kernel. The bandwidth of 2 cM was chosen because it is similar to the average distance between the
121 markers (1.6 cM). To identify genomic islands with both high F_{ST} and d_{XY} , *fastsimcoal2* was used
122 to generate a null distribution of expected F_{ST} and d_{XY} values (i.e. without selection) that
123 incorporated a demographic scenario (Papadopoulos *et al.* 2019) and the position of markers in the
124 genetic map. Under the best fitting *fastsimcoal2* model (a model with initial strong gene flow
125 followed by a reduced gene flow, model 5 in Papadopoulos *et al.* 2019; see Table S1 for parameters),
126 we simulated the same number of 190 bp DNA fragments as contained in the genetic map with the
127 positions preserved by separating simulated loci by the same recombination distances as in the map
128 (i.e., recombination rate between loci varied across the genome). Within fragments, recombination
129 was fixed at the genome wide average (6.85×10^{-9} base⁻¹ generation⁻¹). Each chromosome was
130 simulated 1,000 times separately. Kernel smoothed F_{ST} values were calculated for each simulation
131 using the methods applied to the observed data above. These data were used to calculate P-values at
132 each centimorgan, and outlier F_{ST} islands were identified at alpha = 0.05. Outlier d_{XY} regions were
133 identified as those positions with d_{XY} values in the 90th percentile of the observed data. Observed
134 rather than simulated data was used as the random assignment of mutation in the simulation lead to
135 very broad confidence intervals for d_{XY} . To define the full extent of the high $F_{ST} + d_{XY}$ islands –
136 these islands were joined or extended only if the position next to an $F_{ST} + d_{XY}$ outlier had a high
137 (but not significant) probability of being an F_{ST} outlier (assessed using Hidden Markov Models,
138 HMM) and also coincided with a region of high d_{XY} . To do this, F_{ST} P-values were converted into
139 z-scores using *qnorm* and three hidden states were fitted to detect regions of the genome with low,
140 intermediate and high probabilities of belonging to an outlier region. For each state, a Gaussian

141 distribution of the z-scores was assumed. Means and standard deviations for each hidden state, as
142 well as the transition matrix defining probabilities of transferring from one state to another, were all
143 estimated from the data. Direct transitions from low to high states were not permitted. Parameters
144 were estimated using the Baum-Welch algorithm and the probable sequence of hidden states was
145 determined from the data and parameter estimates using the Verbiti algorithm. The results of the
146 HMM procedure were only used to define the size of the regions identified at $P < 0.05$, rather than
147 locate the position of islands. An island was only extended when an adjacent position (i) was
148 assigned the high F_{ST} state by the HMM and (ii) was an outlier d_{XY} position.

149

150 ESTIMATION OF RECOMBINATION RATE

151 To estimate recombination rates in genomic islands versus the rest of the genome, we assembled a
152 draft genome of *Howea*. We estimated the genome size of *H. forsteriana* and *H. belmoreana*
153 following the one-step flow cytometry procedure described by Doležel *et al.* (2007). Then, a
154 shotgun genome assembly was performed for *H. forsteriana*. A total of 432.98 Gigabases (Gb) of
155 cleaned, paired-end, Illumina reads (49-150 bp reads, insert sizes = 170 bp, 250 bp, 800 bp, 2
156 kilobases (kb), 5 kb, 10 kb and 20 kb) were assembled into genomic contigs using *SOAPdenovo*
157 (Luo *et al.* 2012). *SSPACE* (Boetzer *et al.* 2011) was then used to extend and scaffold contigs.
158 Summary statistics for the shotgun assembly are provided in the supplementary material (Table S2).
159 *BUSCO* (Simão *et al.* 2015) analysis was performed in genome mode using the Embryophyta
160 BUSCOs (Benchmarking Universal Single-Copy Orthologs) to assess genome completeness.
161 Consensus sequences of the ddRAD markers included in the genetic map were mapped to genomic
162 scaffolds using *BLASTn* (Camacho *et al.* 2009), retaining only the best hits. As suggested by Tang
163 *et al.* (2015), scaffolds ($n = 3,980$ and total length = 0.42 Gb) were ordered based on the average
164 map location of the ddRAD markers for each scaffold. The physical length of each chromosome
165 was calculated using the proportion of the total length of scaffolds (0.42 Gb) that mapped to that
166 chromosome. As only 13.3% of the genome is covered by our scaffolds, we then estimated the
167 length of that chromosome as the corresponding proportion of the total genome size of *H.*
168 *forsteriana* (estimated here as 3.15 Gb). Finally, we calculated the recombination rate as the genetic
169 distance from the map divided by the estimated physical length of a given genomic region as above
170 (chromosomes and genomic islands) in 10 cM sliding windows.

171

172 GENE CONTENT IN GENOMIC ISLANDS

173 To assign transcripts from the *Howea* reference transcriptome (Dunning *et al.* 2016) to genomic
174 scaffolds, *BLASTn* was used with $max_target_seqs=1$ and an E-value cut-off of 1×10^{-20} . Only the
175 highest scoring match for each transcript was retained. Using transcriptome data from Dunning *et*

176 *al.* (2016), the proportions of transcripts showing evidence of differential expression or signatures
177 of selection within and outside speciation islands were compared using Fisher's Exact Tests. This
178 was done using highly differentiated genes ($F_{ST} > 0.8$), genes with evidence for positive selection
179 ($d_N/d_S > 1$), and differentially expressed genes in any tissue (Dunning *et al.* 2016). The transcripts
180 from Dunning *et al.* (2016) were mapped to genomic scaffolds using *BLAT* with default settings
181 (Kent 2002). Alignments were then filtered to include only the best hit for each transcript and
182 alignments covering 80% of the transcript. Filtered *BLAT* alignments were then converted to
183 *AUGUSTUS* hints (Stanke *et al.* 2006). *AUGUSTUS* was used to predict genes in the genomic
184 scaffolds, using the transcript-derived hints and annotation training files from *Zea mays* using the
185 following settings: no UTR prediction, no in-frame stop codons, and gene prediction on both
186 strands. The resulting predicted amino acid sequences were *BLASTp*-searched against the
187 *Arabidopsis thaliana* proteome (Araport11_genes.201606.pep downloaded on 31/01/17) and only
188 the best scoring hit from each predicted amino acid sequence was retained. Gene ontology (GO)
189 enrichment for genomic islands was compared to all scaffolded transcripts; this was performed for
190 both transcriptome-based (Dunning *et al.* 2016) and the above *AUGUSTUS*-based genome
191 annotations. To test for enrichment of GO terms among genes within particular genomic islands we
192 used the R package *TopGO* (Alexa *et al.* 2006) using the "elim" algorithm and Fisher's Exact tests
193 to assess significance. Preliminary assessment of gene functions in genomic islands was made from
194 The Arabidopsis Information Resource (TAIR) descriptions of gene functions, GO terms and
195 associated references. Further published records of functional assessments were acquired from the
196 TAIR known phenotypes database (<https://www.arabidopsis.org>), the drought stress genes database
197 (http://pgsb.helmholtz-muenchen.de/droughtdb/drought_db.html) and the flowering interactive
198 database (<http://www.phytosystems.ulg.ac.be/florid/>). Finally, systematic web searches were
199 performed using gene names with and without the terms "stress" and "flowering", given the
200 speciation scenario for *Howea* (Fig. 1).

201

202 **Results and discussion**

203

204 GENE FLOW AND GENOMIC DIFFERENTIATION

205 The linkage map contains 3,772 ddRAD loci ordered onto 16 linkage groups corresponding to the
206 16 pairs of chromosomes in *Howea* (Savolainen *et al.* 2006) and spanning 2,399 cM (0.70 cM/Mb
207 or 1.42 Mb/cM; Fig. 2 and S2, Table S3). Across the map, we observed a positive correlation
208 between F_{ST} and d_{XY} ($p < 0.0001$, $r^2 = 0.18$; Figs. S3 and S4), which, in these relatively recently
209 diverged species, may be an indication that gene flow has played a role in shaping genomic
210 differentiation. To characterise the genomic landscape, F_{ST} and d_{XY} were calculated for 1,498 high-

211 quality ddRAD loci in the map, which were present in both species (genome wide, $F_{ST} = 0.46$, d_{XY}
212 $= 7.6 \times 10^{-3}$). Genetic differentiation during sympatric speciation should be substantially greater for
213 loci that have been subject to divergent selection than for loci in neutral regions (Wu 2001). In the
214 course of speciation with gene flow, genomic regions in proximity with those barrier loci that are
215 the target of selection may experience reduced effective gene flow. Meanwhile, the rest of the
216 genome would still be subject to the homogenising effects of genetic exchange (Nosil *et al.* 2008;
217 Via & West 2008; Soria-Carrasco *et al.* 2014). This may lead to a pattern of elevated differentiation
218 (F_{ST}) and divergence (d_{XY}) in regions containing barrier loci compared to the rest of the genome
219 (Hohenlohe *et al.* 2010; Ellegren *et al.* 2012; Nadeau *et al.* 2012; Martin *et al.* 2013; Renaut *et al.*
220 2013; Poelstra *et al.* 2014). These patterns of heterogeneous genomic differentiation have been used
221 in attempts to identify regions of the genome that harbour barrier loci responsible for adaptation and
222 speciation (Ellegren *et al.* 2012; Nadeau *et al.* 2012; Martin *et al.* 2013; Poelstra *et al.* 2014).
223 However, there are several complicating factors that may mean that these regions do not act as
224 barriers to gene flow (see sections below for discussion of these; Noor & Bennett 2010; Turner &
225 Hahn 2010; Cruickshank & Hahn 2014; Ravinet *et al.* 2017). Here, high- F_{ST} islands (mean $F_{ST} =$
226 0.87 , range = $0.64 - 0.99$, mean $d_{XY} = 9.9 \times 10^{-3}$, range = $5.0 \times 10^{-3} - 1.7 \times 10^{-2}$) were numerous (38
227 islands), relatively small (mean size = 1.7 cM, range = $1 - 5$ cM) and accounted for 3.3% of the
228 genome (total length = 80 cM; Table S4). In contrast, we detected only eight islands with both
229 higher F_{ST} and d_{XY} (high- $F_{ST}+d_{XY}$) than the rest of the genome (mean $F_{ST} = 0.88$, range = $0.58 -$
230 0.98 , mean $d_{XY} = 1.5 \times 10^{-2}$, range = $1.2 \times 10^{-2} - 2.0 \times 10^{-2}$; Welch's t-test, $P < 0.0001$), which were
231 located on seven pairs of chromosomes. These high- $F_{ST}+d_{XY}$ genomic islands were, on average,
232 marginally larger (mean size = 2.38 cM, range = $1 - 4$ cM; Mann-Whitney U test, $P = 0.05$) than
233 other high- F_{ST} islands, and represented only 0.8% of the genome (19 cM, Table S5). A permutation
234 test showed that high- $F_{ST}+d_{XY}$ islands were not the result of high- F_{ST} and high- d_{XY} positions co-
235 occurring by chance ($P < 0.0001$). These high- $F_{ST}+d_{XY}$ islands are more likely to have been
236 involved in speciation in the face of gene flow than islands with high- F_{ST} but no elevation in d_{XY}
237 (Hohenlohe *et al.* 2010; Ellegren *et al.* 2012; Nadeau *et al.* 2012; Martin *et al.* 2013; Renaut *et al.*
238 2013; Poelstra *et al.* 2014). In both species, nucleotide diversity (π) was significantly lower in high-
239 F_{ST} islands than the genome average (Table S6) as has been observed in other plants (Chapman *et*
240 *al.* 2016), but was only lower in high- $F_{ST}+d_{XY}$ islands for *H. forsteriana*. In seven out of eight of
241 high- $F_{ST}+d_{XY}$ islands, π was substantially lower in *H. forsteriana* than in *H. belmoreana*, a possible
242 indication of a selective sweep having taken place in this species. The generally small size of high-
243 $F_{ST}+d_{XY}$ islands indicates that these islands did not expand gradually over time, as would be
244 expected under divergence hitchhiking theory when gene flow is ongoing (Via 2009; Feder *et al.*
245 2012; Rafajlović *et al.* 2016). Our results contrast with those in a comparable analysis of another

246 case of sympatric speciation, i.e., the cichlids of lake Massoko in Tanzania (Malinsky *et al.* 2015).
247 In a whole genome analysis of these fish, and measuring F_{ST} and d_{XY} as here, 55 high- $F_{ST}+d_{XY}$
248 islands were identified. This is substantially more than in the palms here and from a much smaller
249 genome. Similar numbers of islands were found in flycatchers and many more in other systems
250 (Ellegren *et al.* 2012; Renaut *et al.* 2013; Soria-Carrasco *et al.* 2014). This is likely to be, in part,
251 due to the resolution of our map as we have probably missed finer scale islands ($< 1\text{cM}$). However,
252 it is noteworthy that in the Massoko cichlids, 27 islands formed clusters extending 5 - 45 cM across
253 five linkage groups, which are larger than the islands detected in *Howea*, suggesting the resolution
254 we use may be sufficient to detect a substantial proportion of the larger islands in our system.

255 An alternative explanation for high- $F_{ST}+d_{XY}$ islands has been proposed recently (Guerrero & Hahn
256 2017). Guerrero and Hahn showed that these regions can be the result of balanced polymorphisms
257 in the ancestral population that have been ‘sieved’ by the speciation process when different alleles
258 are fixed in each descendent population. Because ancestral balanced polymorphisms have had
259 longer to accumulate divergence than those that only diverged following speciation, this process is
260 expected to have the most pronounced effect early in speciation ($t < 2N_e$; where t = divergence time
261 and N_e = effective population size). If sieved polymorphisms are responsible for these islands,
262 then d_{XY} in these regions should substantially exceed the expected level of d_{XY} based on the time
263 since speciation, which can be calculated as $E(d_{XY}) = 2\mu t + \Theta_{ANC}$ (where μ = the neutral mutation
264 rate and Θ_{ANC} = the ancestral level of diversity). Using respective estimates of t and μ of 266,136
265 and 1.3×10^{-8} from (Papadopulos *et al.* 2019) and assuming $\Theta_{ANC} = 0$ (because of the bottleneck
266 caused by long-distance colonisation of LHI), we arrive at an expected d_{XY} of 6.9×10^{-3} . This
267 differs from the level of d_{XY} estimated from our map by only 0.0007, which may constitute the
268 contribution of ancestral polymorphism to our estimate. Alternatively, this small discrepancy may
269 arise if our estimate of t is wrong by approximately 100,000 years (within the 95% CI of t) or if our
270 d_{XY} estimate is derived only from the subset of the data used for the demographic inference that was
271 also included in the map. These estimates are substantially lower than our mean observed d_{XY} for
272 high- $F_{ST}+d_{XY}$ islands (1.5×10^{-2}), but similar to that of the high- F_{ST} only islands. These data may
273 point to a role for sieved balanced polymorphisms in the origin of our high- $F_{ST}+d_{XY}$ islands, and
274 that sympatric speciation may have been reliant on existing genetic variation in the ancestral
275 population. However, we cannot rule out the possibility that some of these high- $F_{ST}+d_{XY}$ regions
276 may contain sieved polymorphisms that did not play a direct role in the speciation process.

277 278 HIGH- F_{ST} ISLANDS ARE IN REGIONS OF LOW RECOMBINATION

279 Whole genome shotgun sequencing for *H. forsteriana* produced 432.98 Gb of Illumina reads (126x
280 coverage), which assembled into a total length of 3.15 Gb (contig N50 = 3783, scaffold N50 =

281 37,986; Table S2), similar to the genome size estimated from flow cytometry: For *H. forsteriana*,
282 $1C = 3.50 \pm 0.01$ pg ($3,423 \pm 9.78$ Mb); for *H. belmoreana*, $1C = 3.08 \pm 0.02$ pg ($3,012.24 \pm 19.56$
283 Mb). *BUSCO* (Simão *et al.* 2015) analysis of the assembled genome found that 73.2% of BUSCOs
284 were complete.

285 In four of eight high- $F_{ST}+d_{XY}$ islands, the genetic distance (cM) per Mb was lower, i.e.
286 recombination rate was lower, than the average rate for the rest of the chromosome where the island
287 was located, but no different from a random draw (Table S3 and S5, sign test, $P = 0.5$). As a whole,
288 high- $F_{ST}+d_{XY}$ islands did not have significantly lower estimated recombination rates than the rest of
289 the genome (Fig. 3, Welch's t-test, $P = 0.39$), but high- F_{ST} differentiation islands did ($P < 0.0001$).
290 In line with the findings in *Howea*, a recent analysis of sympatric populations of divergent
291 stickleback ecotypes showed that signatures of adaptation were considerably more frequent in
292 regions of low recombination when compared to the same ecotype in sympatry or parallel and
293 divergent ecotypes in allopatry (Samuk *et al.* 2017). It has been proposed that limited marker
294 resolution can result in a reduced ability to detect islands outside regions of low recombination
295 (Lowry *et al.* 2017). Given the resolution of our data this is a possibility. However, not all of the
296 high- F_{ST} only islands detected fall within regions of low recombination and our null model
297 explicitly accounts for the recombination distance between markers, suggesting this is unlikely to be
298 the case. Furthermore, Samuk *et al.* (2017) compared whole genome and 'genotyping by
299 sequencing' and found that the pattern of ecotype-associated divergence correlated with
300 recombination rate was consistent between datasets, and therefore was not an artefact of low marker
301 density. In addition, our high- $F_{ST}+d_{XY}$ islands are not associated with low recombination, indicating
302 that their detection was not an artefact of limited marker density.

303 The association of high- F_{ST} only islands with low recombination could be the result of
304 linked selection (either background selection or hitchhiking) (Burri *et al.* 2015). If genomic
305 diversity was largely shaped by linked selection, we would expect a positive correlation between π
306 and recombination rate; in fact, the opposite is observed across the whole genome (Fig. 4) as well as
307 within both high- F_{ST} and high- $F_{ST}+d_{XY}$ islands (Fig S5). Also, d_{XY} was negatively correlated with
308 recombination rate (Fig. 4, $P < 0.0001$) - a pattern that was also observed in sympatric stickleback
309 ecotypes and interpreted as a joint effect of gene flow and divergent selection (Samuk *et al.* 2017).
310 These findings are consistent with a limited role for linked selection in the evolution of
311 heterogeneous differentiation in *Howea*. Instead, high- F_{ST} only islands are more likely to have
312 arisen as a product of selection after speciation.

313

314 STRESS AND FLOWERING TIME GENES ARE PRESENT IN SPECIATION ISLANDS

315 We detected 37 genes in high- $F_{ST}+d_{XY}$ islands, 19 of which could be annotated by comparison to
316 the *Arabidopsis* Araport11 protein sequences. An additional 233 genes were located in high- F_{ST}
317 only islands, of which we annotated 120. In total 5,309 genes were assigned to the genetic map, of
318 which 3,020 were annotated, including 2,844 with GO terms. We then examined whether these
319 islands were enriched for any GO terms. There was an excess of genes involved in responses to
320 abiotic stimuli and catabolism of organic compounds in our annotated 120 (Table S7). We also
321 evaluated whether genes that were found to be potentially involved in *Howea* speciation by
322 Dunning *et al.* (2016) were present in our islands. Out of 2,250 such candidate genes that were
323 included on our genetic map, 19 were found in high- $F_{ST}+d_{XY}$ islands (Table S8), although this did
324 not represent a higher proportion than expected by chance (Fisher's exact test, $P = 0.863$). Note that
325 4,598 candidate genes from Dunning *et al.* (2016) were not found on the map, and these could still
326 have been important during speciation. Furthermore, it may be that the transcriptome-derived
327 candidate genes (Dunning *et al.* 2016) are regulated by genes within our high- $F_{ST}+d_{XY}$ islands.
328 Alternatively, it is possible that some candidates were not involved in speciation, but diverged
329 subsequently.

330 Finally, we performed a systematic review of the known functions of the 19 annotated genes
331 in high- $F_{ST}+d_{XY}$ islands. We could ascribe 13 of these genes with functions relevant to the
332 speciation scenario, that is, environmental stresses (including those stemming from soil preferences)
333 and flowering time (Fig. 1 and Table S9). Three genes were linked to salt stress, four to drought
334 stress, two to alterations in flowering time, three to osmotic stress, two to cold and three to light
335 stresses (references in Table S9). High- $F_{ST}+d_{XY}$ islands No. 3.1, 5.1, 12.1 and 15.1 contained
336 multiple genes with relevant functions (Table S9), and it is noteworthy that both islands 3.1 and
337 15.1 contained genes with $F_{ST} > 0.9$ (Dunning *et al.* 2016) as well as a combination of genes
338 involved in both environmental responses and flowering time control. These are good candidate
339 genes for adaptation and speciation as the habitat that *H. forsteriana* occupies is characterised by
340 low soil moisture and increased salt, light and wind exposure (Papadopoulos *et al.* 2019).

341

342 REFERENCES

343

344 Alexa, A., Rahnenführer, J. & Lengauer, T. (2006). Improved scoring of functional groups from
345 gene expression data by decorrelating GO graph structure. *Bioinformatics* 22: 1600–1607.

346 Babik, W., Butlin, R.K., Baker, W.J., Papadopoulos, A.S.T., Boulesteix, M., Anstett, M.C., *et al.*
347 (2009). How sympatric is speciation in the *Howea* palms of Lord Howe Island? *Mol. Ecol.* 18:
348 3629–3638.

349 Boetzer, M., Henkel, C. V., Jansen, H.J., Butler, D. & Pirovano, W. (2011). Scaffolding pre-

350 assembled contigs using SSPACE. *Bioinformatics* 27: 578–579.

351 Broman, K.W., Wu, H., Sen, Å. & Churchill, G.A. (2003). R/qtl: QTL mapping in experimental
352 crosses. *Bioinformatics* 19: 889–890.

353 Burri, R., Nater, A., Kawakami, T., Mugal, C.F., Olason, P.I., Smeds, L., *et al.* (2015). Linked
354 selection and recombination rate variation drive the evolution of the genomic landscape of
355 differentiation across the speciation continuum of Ficedula flycatchers. *Genome Res.* 25:
356 1656–1665.

357 Camacho, C., Coulouris, G., Avagyan, V., Ma, N., Papadopoulos, J., Bealer, K., *et al.* (2009).
358 BLAST plus: architecture and applications. *BMC Bioinformatics* 10: 1.

359 Catchen, J.M., Amores, A., Hohenlohe, P., Cresko, W. & Postlethwait, J.H. (2011). Stacks:
360 Building and Genotyping Loci De Novo From Short-Read Sequences. *G3 Genes, Genomes,*
361 *Genet.* 1: 171–182.

362 Chapman, M.A., Hiscock, S.J. & Filatov, D.A. (2016). The genomic bases of morphological
363 divergence and reproductive isolation driven by ecological speciation in Senecio (Asteraceae).
364 *J. Evol. Biol.* 29: 98–113.

365 Coyne, J.A. (2011). Speciation in a small space. *Proc. Natl. Acad. Sci.* 108: 12975–12976.

366 Cruickshank, T.E. & Hahn, M.W. (2014). Reanalysis suggests that genomic islands of speciation
367 are due to reduced diversity, not reduced gene flow. *Mol. Ecol.* 23: 3133–3157.

368 Doležel, J., Greilhuber, J. & Suda, J. (2007). Estimation of nuclear DNA content in plants using
369 flow cytometry. *Nat. Protoc.* 2: 2233–44.

370 Doyle, J.J. & Doyle, J.L. (1987). A rapid DNA isolation procedure for small amounts of fresh leaf
371 tissue. *Phytochem. Bull.* 19: 11–15.

372 Dunning, L.T., H. Hipperson, Baker, W.J., Butlin, R.K., Devaux, C., Hutton, I., *et al.* (2016).
373 Ecological speciation in sympatric palms: 1. Gene expression, selection and pleiotropy. *J.*
374 *Evol. Biol.* 29: 1472–1487.

375 Ellegren, H., Smeds, L., Burri, R., Olason, P.I., Backstrom, N., Kawakami, T., *et al.* (2012). The
376 genomic landscape of species divergence in Ficedula flycatchers. *Nature* 491: 756–760. Nature
377 Publishing Group, a division of Macmillan Publishers Limited. All Rights Reserved.

378 Feder, J.L., Egan, S.P. & Nosil, P. (2012). The genomics of speciation-with-gene-flow. *Trends*
379 *Genet.* 28: 342–350. Elsevier Trends Journals.

380 Guerrero, R.F. & Hahn, M.W. (2017). Speciation as a sieve for ancestral polymorphism. *Mol. Ecol.*
381 1–7.

382 Hipperson, H., Dunning, L.T., Baker, W.J., Butlin, R.K., Hutton, I., Papadopoulos, A.S.T.T., *et al.*
383 (2016). Ecological speciation in sympatric palms: 2. Pre- and post-zygotic isolation. *J. Evol.*
384 *Biol.* 29: 2143–2156.

385 Hohenlohe, P.A., Bassham, S., Etter, P.D., Stiffler, N., Johnson, E.A. & Cresko, W.A. (2010).
386 Population genomics of parallel adaptation in threespine stickleback using sequenced RAD
387 tags. *PLoS Genet* 6: e1000862. Public Library of Science.

388 Keenan, K., McGinnity, P., Cross, T.F., Crozier, W.W. & Prodöhl, P.A. (2013). diveRsity: An R
389 package for the estimation and exploration of population genetics parameters and their
390 associated errors. *Methods Ecol. Evol.* 4: 782–788.

391 Kent, W.J. (2002). BLAT — The BLAST -Like Alignment Tool. *Genome Res.* 12: 656–664.

392 Lowry, D.B., Hoban, S., Kelley, J.L., Lotterhos, K.E., Reed, L.K., Antolin, M.F., *et al.* (2017).
393 Breaking RAD: an evaluation of the utility of restriction site-associated DNA sequencing for
394 genome scans of adaptation. *Mol. Ecol. Resour.* 17: 142–152.

395 Luo, R., Liu, B., Xie, Y., Li, Z., Huang, W., Yuan, J., *et al.* (2012). SOAPdenovo2: an empirically
396 improved memory-efficient short-read de novo assembler. *Gigascience* 1: 18.

397 Malinsky, M., Challis, R.J., Tyers, A.M., Schiffels, S., Terai, Y., Ngatunga, B.P., *et al.* (2015).
398 Genomic islands of speciation separate cichlid ecomorphs in an East African crater lake.
399 *Science* (80-.). 350: 1493–1498.

400 Martin, S.H., Dasmahapatra, K.K., Nadeau, N.J., Salazar, C., Walters, J.R., Simpson, F., *et al.*
401 (2013). Genome-wide evidence for speciation with gene flow in *Heliconius* butterflies.
402 *Genome Res.* 23: 1817–1828.

403 Nadeau, N.J., Whibley, A., Jones, R.T., Davey, J.W., Dasmahapatra, K.K., Baxter, S.W., *et al.*
404 (2012). Genomic islands of divergence in hybridizing *Heliconius* butterflies identified by
405 large-scale targeted sequencing. *Philos. Trans. R. Soc. B Biol. Sci.* 367: 343–353.

406 Nei, M. (1987). *Molecular evolutionary genetics*. Columbia university press.

407 Noor, M.A.F. & Bennett, S.M. (2010). Islands of speciation or mirages in the desert? Examining the
408 role of restricted recombination in maintaining species. *Heredity (Edinb)*. 103: 439–444.

409 Nosil, P., Egan, S.P. & Funk, D.J. (2008). Heterogeneous genomic differentiation between walking-
410 stick ecotypes: ‘isolation-by-adaptation’ and multiple roles for divergent selection. *Evolution*
411 (*N. Y.*) 62: 316–336.

412 Papadopulos, A.S.T., Baker, W.J., Crayn, D., Butlin, R.K., Kynast, R.G., Hutton, I., *et al.* (2011).
413 Speciation with gene flow on Lord Howe Island. *Proc. Natl. Acad. Sci. U. S. A.* 108: 13188–
414 13193.

415 Papadopulos, A.S.T., Igea, J., Smith, T.P., Osborne, O., Dunning, L., Turnbull, C., *et al.* (2019).
416 Ecological speciation in sympatric palms: 4. Demographic analyses support that *Howea* did
417 speciate in the face of high gene flow. *Evolution (in revision)*.

418 Papadopulos, A.S.T., Kaye, M., Devaux, C., Hipperson, H., Lighten, J., Dunning, L.T., *et al.*
419 (2014). Evaluation of genetic isolation within an island flora reveals unusually widespread

420 local adaptation and supports sympatric speciation. *Philos. Trans. R. Soc. B Biol. Sci.* 369:
421 20130342.

422 Papadopulos, A.S.T., Price, Z., Devaux, C., Hipperson, H., Smadja, C.M., Hutton, I., *et al.* (2013).
423 A comparative analysis of the mechanisms underlying speciation on Lord Howe Island. *J.*
424 *Evol. Biol.* 26: 733–745.

425 Poelstra, J.W., Vijay, N., Bossu, C.M., Lantz, H., Ryll, B., Müller, I., *et al.* (2014). The genomic
426 landscape underlying phenotypic integrity in the face of gene flow in crows. *Science (80-.)*.
427 344: 1410–1414.

428 R_Development_Core_Team. (2019). R: a language and environment for statistical computing. R
429 Foundation for Statistical Computing, Vienna, Austria.

430 Rafajlović, M., Emanuelsson, A., Johannesson, K., Butlin, R.K. & Mehlig, B. (2016). A universal
431 mechanism generating clusters of differentiated loci during divergence-with-migration.
432 *Evolution (N. Y.)*. 70: 1609–1621.

433 Ravinet, M., Faria, R., Butlin, R.K., Galindo, J., Bierne, N., Rafajlović, M., *et al.* (2017).
434 Interpreting the genomic landscape of speciation: a road map for finding barriers to gene flow.
435 *J. Evol. Biol.* 30: 1450–1477.

436 Renaut, S., Grassa, C.J., Yeaman, S., Moyers, B.T., Lai, Z., Kane, N.C., *et al.* (2013). Genomic
437 islands of divergence are not affected by geography of speciation in sunflowers. *Nat. Commun.*
438 4: 1827.

439 Samuk, K., Owens, G.L., Delmore, K.E., Miller, S.E., Rennison, D.J. & Schluter, D. (2017). Gene
440 flow and selection interact to promote adaptive divergence in regions of low recombination.
441 *Mol. Ecol.* 26: 4378–4390.

442 Savolainen, V., Anstett, M.-C., Lexer, C., Hutton, I., Clarkson, J.J., Norup, M. V., *et al.* (2006).
443 Sympatric speciation in palms on an oceanic island. *Nature* 441: 210–213.

444 Simão, F.A., Waterhouse, R.M., Ioannidis, P., Kriventseva, E. V. & Zdobnov, E.M. (2015).
445 BUSCO: Assessing genome assembly and annotation completeness with single-copy
446 orthologs. *Bioinformatics* 31: 3210–3212.

447 Soria-Carrasco, V., Gompert, Z., Comeault, A.A., Farkas, T.E., Parchman, T.L., Johnston, J.S., *et*
448 *al.* (2014). Stick Insect Genomes Reveal Natural Selection’s Role in Parallel Speciation.
449 *Science (80-.)*. 344: 738–742.

450 Stanke, M., Schöffmann, O., Morgenstern, B. & Waack, S. (2006). Gene prediction in eukaryotes
451 with a generalized hidden Markov model that uses hints from external sources. *BMC*
452 *Bioinformatics* 7: 62.

453 Sundaresan, V. & Alandete-Saez, M. (2010). Pattern formation in miniature: the female
454 gametophyte of flowering plants. *Development* 137: 179–189.

455 Tang, H., Zhang, X., Miao, C., Zhang, J., Ming, R., Schnable, J.C., *et al.* (2015). ALLMAPS:
456 robust scaffold ordering based on multiple maps. *Genome Biol.* 1–15.

457 Turner, T.L. & Hahn, M.W. (2010). Genomic islands of speciation or genomic islands and
458 speciation? *Mol. Ecol.* 19: 848–850.

459 Via, S. (2009). Natural selection in action during speciation. *Proc. Natl. Acad. Sci.* 106: 9939–9946.

460 Via, S. & West, J. (2008). The genetic mosaic suggests a new role for hitchhiking in ecological
461 speciation. *Mol. Ecol.* 17: 4334–4345. Blackwell Publishing Ltd.

462 Weir, B.S. & Cockerham, C.C. (1984). Estimating F-statistics for the analysis of population
463 structure. *Evolution (N. Y.)* 38: 1358–1370. Society for the Study of Evolution.

464 Woodroffe, C.D., Kennedy, D.M., Brooke, B.P. & Dickson, M.E. (2006). Geomorphological
465 evolution of Lord Howe Island and carbonate production at the latitudinal limit to reef growth.
466 *J. Coast. Res.* 22: 188–201. Coastal Education and Research Foundation.

467 Wu, C.I. (2001). The genic view of the process of speciation. *J. Evol. Biol.* 14: 851–865.

468

469

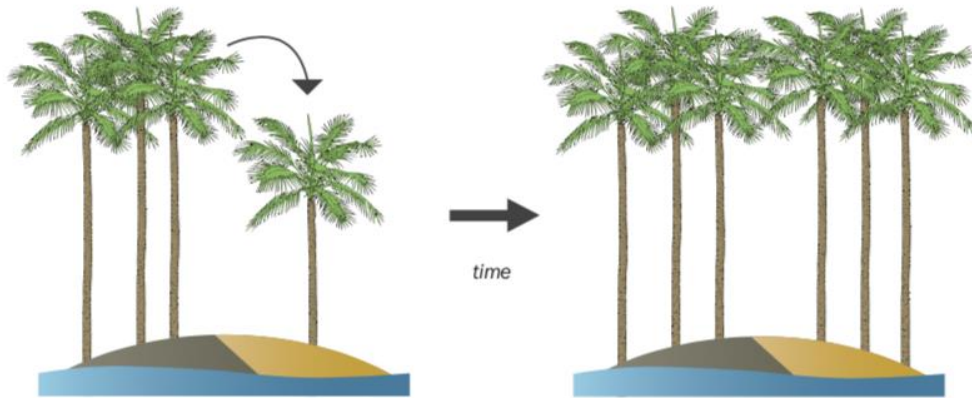
470

471

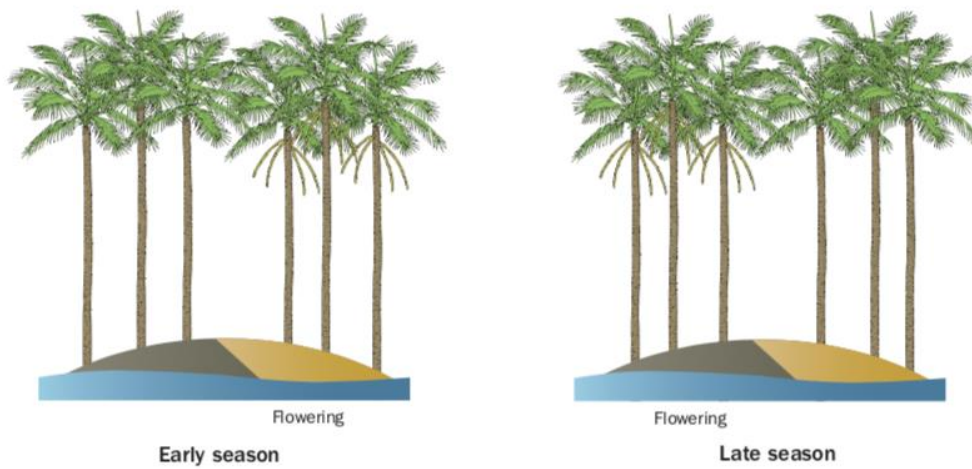
472

473

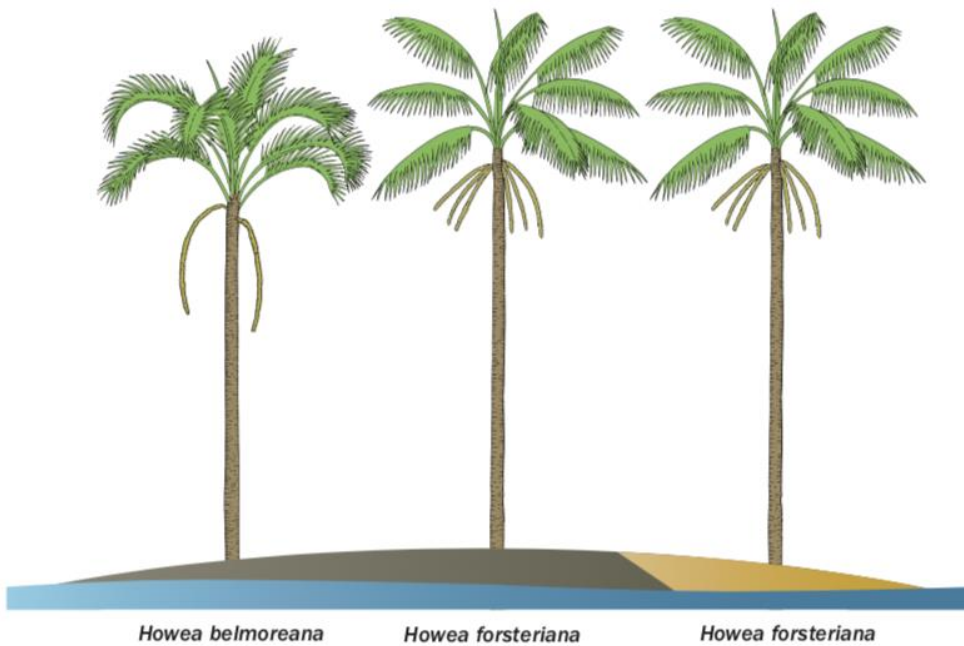
1. Ancestral *Howea* colonises calcarenite soils (disruptive selection)



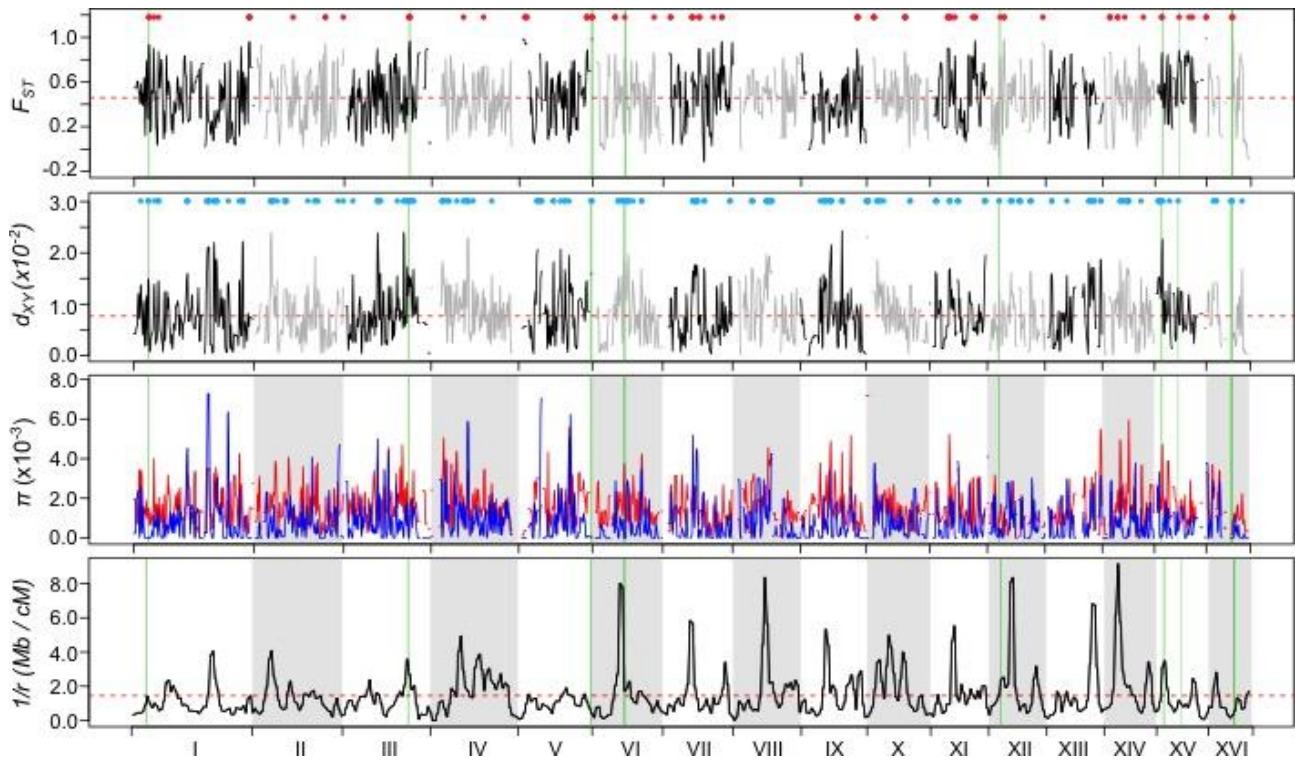
2. Assortative mating via flowering time differences promotes species divergence (speciation)



3. Speciation is followed by further phenotypic, physiological and genetic divergence



475 **Fig. 1** Hypothesised speciation scenario for *Howea*. (1) Lord Howe Island is composed of two main
476 soil types, volcanic (the initial soil type; dark brown) and calcareous soils (subsequent calcarenite
477 deposits; light brown). An ancestral *Howea* colonised Pleistocene calcarenite deposits from
478 volcanic soils, resulting in disruptive selection via adaptation to environmental stresses (e.g.,
479 stemming from soil preferences) and triggering flowering time differences. (2) Assortative mating
480 via displacement of flowering phenology promoted reproductive isolation. (3) Further divergence
481 arose after speciation. Today, the curly palm, *H. belmoreana*, grows on volcanic soils, has erect
482 leaflets, a single spike per inflorescence, and flowers late in the season. The kentia palm, *H.*
483 *forsteriana*, has colonised both calcareous and volcanic soils, has pendulous leaflets, multiple
484 spikes per inflorescence, and it flowers earlier in the season; it is also one of the world's most
485 commonly traded houseplants.
486



489

490

491

492

493

494

495

496

497

498

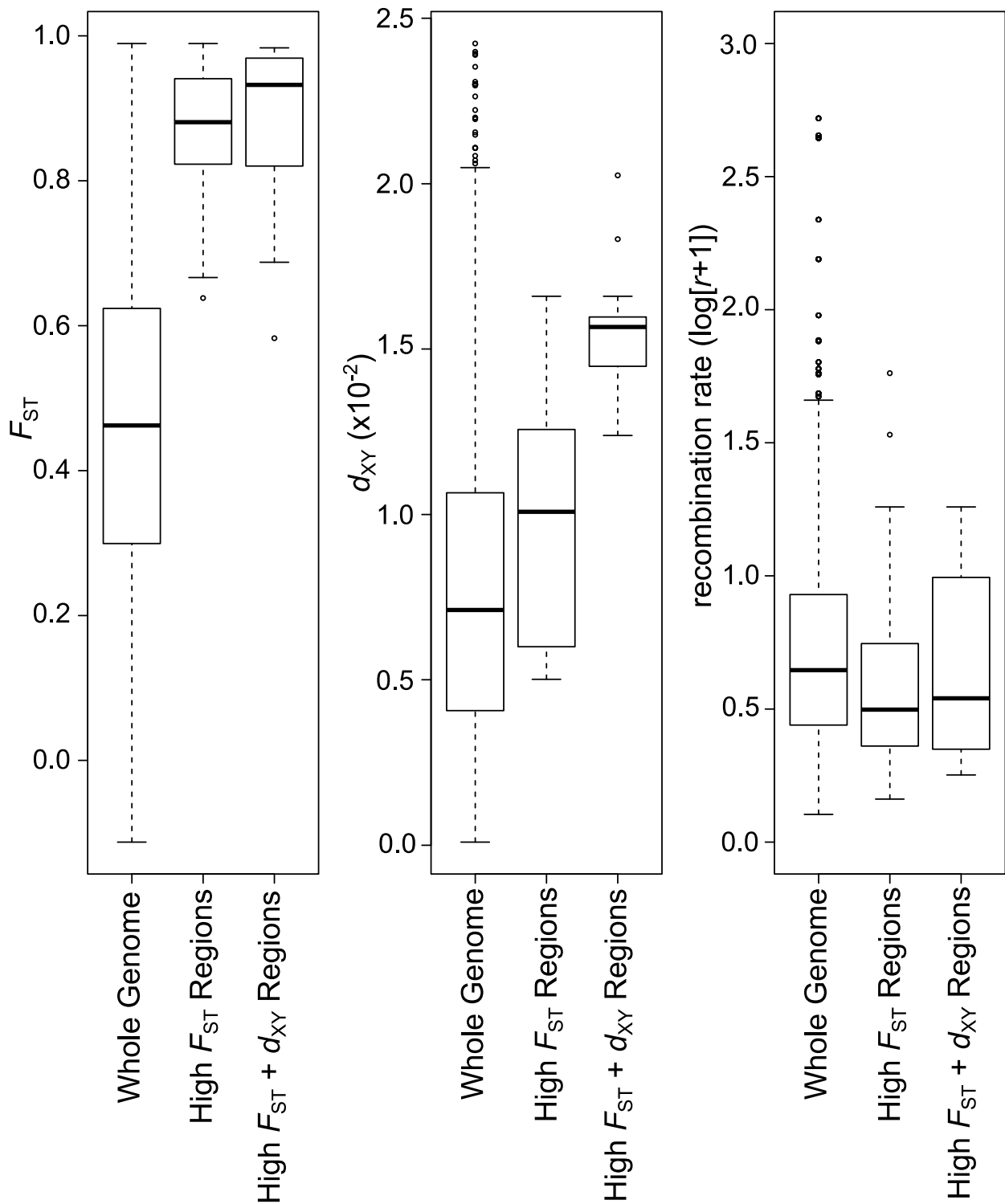
499

500

501

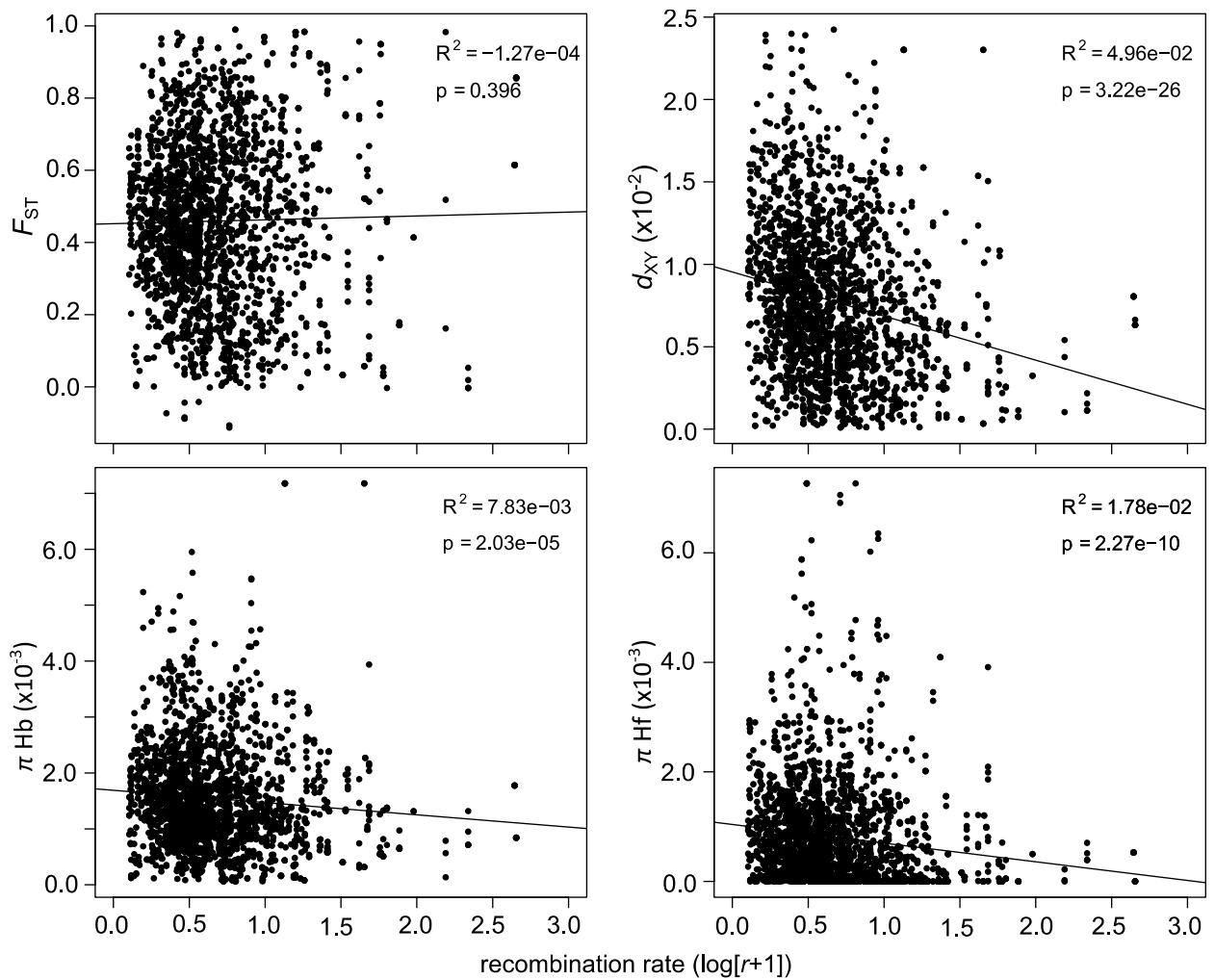
502

Fig. 2 Genomic divergence between *H. belmoreana* and *H. forsteriana*. The x-axis denotes the genomic order of ddRAD markers on each chromosome. Chromosomes are ordered by length in cM. In the F_{ST} and d_{XY} plots (top two panels) kernel smoothed values of F_{ST} and d_{XY} on each chromosome are shown in alternately black and grey for adjacent chromosomes, coloured dots denote the positions of outlier positions (red = F_{ST} and blue = d_{XY}), dashed red lines denote the genome average. Vertical green bars signify the positions of the 15 high- $F_{ST}+d_{XY}$ islands more likely involved in sympatric speciation, and red dots are the high- F_{ST} only islands more likely to have occurred post-speciation (see text). Genetic diversity (π) for *H. belmoreana* and *H. forsteriana* are shown by red and blue lines, respectively. The lower panel shows the recombination rate in 10cM windows. High- F_{ST} and high- $F_{ST}+d_{XY}$ islands appear to be associated with regions of low recombination (i.e., low cM per Mb; high $1/r$), but this association is not statistically significant. Note that genetic diversity is not lower in speciation islands despite low recombination.



503
 504
 505
 506

Fig. 3 Comparison of divergence metrics. Boxplots depict the median (bold line), interquartile range (box), and 1.5 times the interquartile range (whiskers).



507

508 **Fig. 4** Genome wide relationships of recombination rate with population genetic metrics indicate no
 509 role for linked selection in shaping differentiation in *Howea*. Recombination rate was not correlated
 510 with F_{ST} but was negatively correlated with d_{XY} and π in both species.

511

512